Ultramicroscopy 111 (2011) 1239–1246

Contents lists available at ScienceDirect

Ultramicroscopy

journal homepage: www.elsevier.com/locate/ultramic

Transmission electron microscopy at 20 kV for imaging and spectroscopy

U. Kaiser [a,*], J. Biskupek [a], J.C. Meyer [a], J. Leschner [a], L. Lechner [a], H. Rose [a], M. Stöger-Pollach [b], A.N. Khlobystov [c], P. Hartel [d], H. Müller [d], M. Haider [d], S. Eyhusen [e], G. Benner [e]

[a] Central Facility of Electron Microscopy, Group of Electron Microscopy of Materials Science, Ulm University, Albert-Einstein-Allee 11, 89081 Ulm, Germany
[b] University Service Centre for TEM (USTEM), Vienna University of Technology, 1040 Wien, Austria
[c] School of Chemistry, University of Nottingham, University Park, Nottingham NG7 2RD, United Kingdom
[d] CEOS GmbH, Englerstraße 28, 69126 Heidelberg, Germany
[e] Carl Zeiss NTS GmbH, Carl-Zeiss-Strasse 56, 73447 Oberkochen, Germany

ARTICLE INFO

Article history:
Received 22 December 2010
Received in revised form
10 March 2011
Accepted 16 March 2011
Available online 1 April 2011

Keywords:
Low-voltage TEM
Beam damage
High resolution
EELS

ABSTRACT

The electron optical performance of a transmission electron microscope (TEM) is characterized for direct spatial imaging and spectroscopy using electrons with energies as low as 20 keV. The highly stable instrument is equipped with an electrostatic monochromator and a C_S-corrector. At 20 kV it shows high image contrast even for single-layer graphene with a lattice transfer of 213 pm (tilted illumination). For 4 nm thick Si, the 200 reflections (271.5 pm) were directly transferred (axial illumination). We show at 20 kV that radiation-sensitive fullerenes (C_{60}) within a carbon nanotube container withstand an about two orders of magnitude higher electron dose than at 80 kV. In spectroscopy mode, the monochromated low-energy electron beam enables the acquisition of EELS spectra up to very high energy losses with exceptionally low background noise. Using Si and Ge, we show that 20 kV TEM allows the determination of dielectric properties and narrow band gaps, which were not accessible by TEM so far. These very first results demonstrate that low kV TEM is an exciting new tool for determination of structural and electronic properties of different types of nano-materials.

1. Introduction

Aberration corrected transmission electron microscopy (TEM) is currently undergoing revolutionary changes in its ability to image materials at the atomic level using medium energy electrons [1–4]. However, the resolution in the TEM image is often limited by radiation damage rather than by the quality of the instrument [5,6]. The damaging effects include ionization, heating, chemical etching and knock-on displacement of atoms. While ionization and heating depend on the beam current applied to the specimen, knock-on damage depends solely on the energy of the electrons. Therefore, this damage effect can only be avoided by reducing the voltage below the knock-on threshold of the objects under study.

Already in the early days of electron microscopy, more than 45 years ago, attempts were made to visualize biological samples with high contrast in a TEM operating at voltages as low as 6 kV [7]. However, at this time the performance of the microscope was very poor due to the large chromatic aberration. In the following decades, the use of low voltages in TEM was completely abandoned. Recent advances in the design of suitable aberration correctors [1,2] initiated a revival of low-voltage electron microscopy [6,8] spurring world-wide activity. For example, a double C_S aberration corrected low-voltage TEM operating at accelerating voltages between 30 and 60 kV is currently being designed at the National Institute of Advanced Industrial Science and Technology (AIST), Tsukuba, Japan [9]. Very recently, it has been demonstrated that also the Nion UltraSTEM is capable of atomic resolution imaging at 60 kV in STEM mode by virtue of its 3rd-generation C_3/C_5 corrector [10]. These examples illustrate a high level of interest in lower voltage TEM driven by the need to image increasingly complex and delicate structures.

Within the frame of the *S*ub-Ångstrom *L*ow-*V*oltage *E*lectron microscopy (*SALVE*) project, we aim at improving the instrumental resolution by optimizing all components of the *SALVE* microscope and by integrating a new C_C/C_S corrector into the final instrument for electron beam (e-beam) energies down to 20 keV. Our new approach is intended to enhance the specimen resolution given by $d_s=\sqrt{d_i^2+(S/N)^2/DC^2}$ [6] of radiation-sensitive materials by low-voltage operation. The product of tolerable dose D times contrast C is nearly independent of the voltage. Because the contrast increases with decreasing voltage and the required signal-to-noise (S/N) ratio is fixed, we can decrease d_s by going to

* Corresponding author.
E-mail address: ute.kaiser@uni-ulm.de (U. Kaiser).

0304-3991/$ - see front matter © 2011 Elsevier B.V. All rights reserved.
doi:10.1016/j.ultramic.2011.03.012

lower voltages provided that the instrumental resolution limit d_i does not increase [6]. This requirement can be satisfied only by means of a novel C_C/C_S corrector, which compensates for chromatic and spherical aberrations and provides a wide field of view.

Imaging of predominantly knock-on damage sensitive semiconductors, minerals, oxides and organic molecules requires low-voltage. Low-voltage TEM in turn necessitates very thin objects to avoid resolution degradation caused by multiple scattering. For most bulk materials appropriate target preparation methods are necessary to create self-supporting specimens. Present studies are limited to very few materials where conventional preparation techniques can be applied to create electron transparent areas. In contrast, focused ion beam techniques allow TEM specimens to be prepared from almost any material. Such a lamella suitable for high-resolution TEM (HRTEM) observation at 20 kV has to be prepared much thinner than 10 nm. However, using conventional lift-out technique [11] and low-kV Ga milling minimum lamella thicknesses of 20–30 nm are achievable at the best [12]. In addition, demands for homogeneity and absence of surface contamination are not met by these specimen.

Imaging single molecules requires a supporting conductive substrate. We intend to employ graphene, a single-layer graphite [13], as a precisely defined and thinnest possible substrate. Moreover, if its structure is removed from the image by Fourier filtering, the HRTEM image of the free-standing object is obtained [8,14] if bonding effects between molecule and substrate can be neglected. In addition, electrons from the highly conducting substrates might replace ejected electrons of the molecules before bonds break [37].

Analytical low-voltage TEM combines imaging with peculiarities of spectroscopy at low voltages. Especially for valence EELS (VEELS) low e-beam energies are advantageous, as a strong increase in signal to background ratio is observed. This effect is most probably caused by a reduction or avoidance of relativistic energy losses, like Cerenkov losses and light-guided modes [15–17]. Calculations [17] predict the Cerenkov limit for silicon in a range between 15 and 20 kV. The same threshold for germanium is below 5 kV. These results suggest that at 20 kV at least silicon can be studied free of relativistic energy losses. Furthermore, the range of the Coulomb interaction between the incident electron and the electrons of the sample is also reduced at 20 kV resulting in a decreased delocalization width [16]. Since the transferred momentum $\hbar\mathbf{q}_E$ increases for lower electron energies, the resolution of the "inelastic" image also increases as long as aberrations and/or diffraction are not the limiting factors.

In this study, we report for the first time on specifications and applications of the prototype *SALVE* instrument operating at 20 kV accelerating voltage. Our first example shows the capability of the instrument to image e-beam-sensitive fullerene C_{60} molecules. They have been encapsulated in the thinnest and smallest available test-tube, a single-walled carbon nanotube. Defect-free carbon nanotubes are e-beam transparent and structurally stable for infinite time at or below 80 kV [18,19]. The second example demonstrates the analytical potential of the prototype *SALVE* instrument for insulating and/or semiconducting materials by using EELS at 20 kV for investigating the low-loss region of Si and Ge.

2. Experiments

2.1. Instrumental details

The prototype *SALVE* microscope is a monochromated Libra 200 MC with in-column corrected OMEGA filter and imaging CEOS C_S-corrector (CETCOR). For 20 keV electrons the monochromator [20] creates high image contrast at high spatial frequencies: slit widths of 2.5 and 2 μm result in a full width at half maximum (FWHM) of 0.17 and 0.15 eV for the incident electron beam, respectively. The microscope was operated with the OMEGA filter always turned on during all experiments. In imaging mode the energy window (5 eV) of the energy selecting slit was centered around the zero-loss peak. EELS was carried out using a smaller monochromator slit of 1 μm—resulting in an energy FWHM <0.1 eV when measured for 1 s in vacuum. In order to obtain a good signal-to-noise ratio for the EELS data (including both zero-loss peak and plasmon losses) in each experiment 100 single spectra were acquired with 0.2 s exposure time. The spectra were then corrected for energy shifts by drift correlation and subsequently averaged. All images and spectra were recorded by a Gatan $2k\times 2k$ slow scan CCD 16 bit camera, type Ultrascan 1000. The conversion rate of the camera at 20 kV was determined to be 0.5 CCD counts per electron by Faraday cup measurements. Since we need a sufficiently large number of electrons in order to achieve signals above the readout noise of the CCD. the poor conversion rate requires much more electrons for exciting a sufficient number of photons than the ≥ 5 counts per electron for conventional HRTEM in medium voltage operation.

The information limit of the microscope at 20 kV is determined by the combination of image spread and focus spread [21]. The focus spread limit, which comprises the effect of the chromatic aberration and other focus instabilities can be reduced from 0.5 nm without monochromator to 0.25 nm with a reduced energy width of 0.17 eV. The image spread limit, which includes all kinds of lateral noise has been determined to be better than 0.18 nm.

The accelerator design and the alignment of the FEG have been optimized for low-voltage operation. The instrument can cover a voltage range from 20 to 80 kV (200 kV) without any loss in brightness (referred to the extraction voltage). We demonstrate that especially for low beam energies the electrostatic omega principle for monochromatization and the corrected in-column technology are beneficial for filtered images with low energy width and highly resolved spectroscopy.

2.2. Preparation of Si and Ge samples

We used a Zeiss NVision 40 Ar cross-beam microscope equipped with a SEM column, a Ga FIB column, and a focused Ar beam. One micrometer thick lamellas were produced from bulk material by conventional in-situ lift-out technique. They were planarized and thinned to approximately 0.5 μm thickness using 30 kV Ga-ions and low Ga-beam currents (down to 10 pA). Subsequently, a series of rectangular recesses, each about 200 nm deep, was milled into one side of the lamella. Both sides of the lamella were then polished in several steps, decreasing Ga beam voltage (down to 1 kV) to reduce the amorphous layer thickness. Finally residual Ga contamination was removed by polishing with the Ar ion source at 500 V. Using this technique, we obtained Si lamellae with thicknesses down to 4 nm (thickness determined by EELS measurement). Details of the preparation technique are described in [22]. For the EELS experiments, the sample thickness was chosen to be in the range from 0.2 to 0.5 times the mean free path lengths for inelastic scattered electron. This thickness range ensures low plural scattering – which can then be subsequently deconvolved from the spectrum – and a sufficiently high inelastic scattering cross-section.

2.3. Preparation of graphene and C_{60} at DWNT

Graphene membranes were prepared by following the CVD methods for graphene synthesis on nickel substrates [23–25]. The CVD grown graphene sheets were transferred onto commercial TEM grids as described previously [15]. Arc-discharge nanotubes

(*NanoCarbLab*) were heated in air at 520 °C for 20 min to remove adsorbed water and to open their termini. The nanotubes were cooled down to room temperature and without delay combined with a weight equivalent of crystalline fullerene C_{60} (99.9% pure, *SES Research*). The mixture was sealed in a quartz tube in 10^{-4} Pa vacuum and heated at 500 °C for 2 days. The excess of fullerenes was removed from the surface of the nanotubes by extensive washing with carbon disulfide (CS_2). The resultant sample was dried in air. A small amount of C60@DWNT powder (~10 μg) was suspended in 2 ml of methanol using an ultrasonic bath. The suspension was drop-cast onto a lacey-carbon coated TEM grid.

2.4. EELS analysis

The refractive index has been determined from the dielectric function by Kramers–Kronig analysis (KKA) after plural scattering deconvolution. Due to the high dispersion of the spectrometer at 20 kV (0.023 eV/channel), only a small portion of the EELS spectrum can be recorded on the camera. Consequentially, the high-energy end of the spectrum is cut-off so that the intensity of the recorded spectrum does not approach zero. This behavior causes problems when using the conventional Fourier-log deconvolution routine, because any Fourier deconvolution requires a periodic function [26]. A way out of this problem is the matrix deconvolution [27]. After retrieval of the single scattering distribution, conventional KKA can be applied yielding the optical properties.

3. Results

3.1. Characterization of the 20 kV SALVE microscope

The information limit and the axial aberrations of our prototype *SALVE* microscope optimized for 20 kV operation were measured using thin amorphous carbon foils. The results were confirmed by crystalline silicon and graphene samples. Spectroscopy was performed on silicon and germanium.

3.1.1. Information limit

At an energy E_0 of 20 keV, the chromatic aberration coefficient C_C amounts to 1.26 mm (calculation), which is in good agreement with the measured value of (1.2 ± 0.1) mm. This value was determined using $C_C = E_0/\Delta E \ldots \Delta f$, where the change of focus Δf with changed electron energy ΔE was recorded in several steps of 10 eV.

Therefore, without monochromator ($\Delta E = 0.75$ eV, FWHM) the focus spread contribution from the chromatic aberration is limiting the resolution at 0.52 nm (calculated for a contrast of 13.5%), which is supported by a Young's fringes measurement shown in Fig. 1a. Operating the monochromator with a slit width of 2.5 μm ($\Delta E = 0.17$ eV) extends the range of Young's fringes (Fig. 1b). In this case the calculated 13.5%-level is 0.25 nm. Smaller slits at the monochromator did not improve the attainable resolution in terms of Young's fringes because of intensity reasons.

The slightly enhanced visibility of Young's fringes in comparison to the calculated 13.5%-levels has several reasons: "visibility" in a diffractogram is related to a contrast level of about 1%, which is at a factor of $\sqrt[4]{0.5 \ln 100} \approx 1.23$ times higher spatial frequency than the 13.5%-level. The scattering amplitude of the specimen also has to be taken into account, especially at higher spatial frequencies. Finally, non-linear effects due to specimen thickness can increase the visibility beyond the limit set by the focus spread damping envelope [21].

The image spread limit of the instrument was shown to be better than 0.18 nm by applying an illumination tilt of 30 mrad in combination with Young's fringes (Fig. 1c) [21].

3.1.2. Axial aberrations

The only intrinsic axial aberrations up to fifth order for the current *SALVE* microscope with hexapole C_S-corrector (tuned for a small C_C-contribution) are the six-fold astigmatism $A_5 = 15$ mm and the fifth-order spherical aberration $C_5 = 21$ mm (for minimized off-axial coma). The measurements in Table 1 show slightly higher values than calculated. Most probably this is due to calibration limits of magnification and tilt on which the values depend in second and fourth power, respectively.

The intrinsic six-fold astigmatism reaches the $\pi/4$-limit at 27 mrad equivalent to 1/0.31 nm. The measured aberration coefficients (for definitions refer to [29]) in Table 1 violate the $\pi/4$-limit from 20 mrad (1/0.43 nm) on. However, higher order aberrations can partly be compensated by lower order aberrations of the same multiplicity (except for *n*-fold astigmatism). The precision of the measurement indicates that a well-corrected state with partial compensation (measured or compensated aberrations below precision) can be achieved for 27 mrad (1/0.32 nm). Since the second order coma B_2 has one-fold symmetry, its residual phase shift is always partially counterbalanced by a small image displacement. The allowed budget for residual phase shift due to axial coma is by a factor of four larger than estimated by the single-coefficient $\pi/4$-limit [29]. Therefore, the precision of the axial coma measurement as stated in Table 1 is sufficient for a maximum aperture angle of 27 mrad.

This shows that, in a TEM equipped with a monochromator, the hexapole C_S-corrector can be used for phase contrast imaging at 20 kV up to the limit set by the intrinsic six-fold astigmatism.

The envisioned new C_C/C_S-corrector for the final *SALVE* microscope will have correction tools up to axial aberrations of fourth order. Intrinsic aberrations of fifth order are by design sufficiently

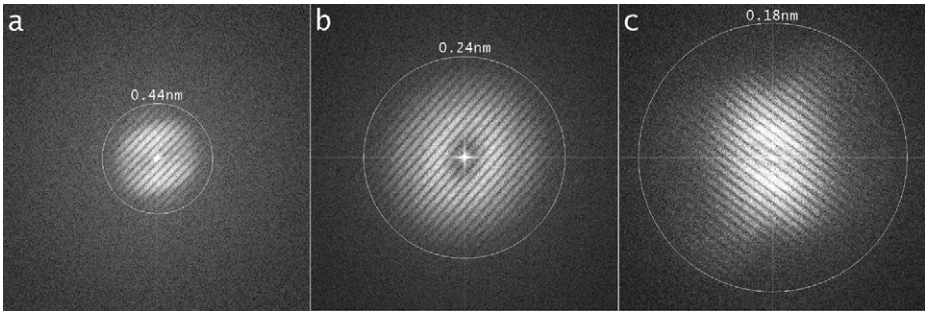

Fig. 1. Diffractograms with Young's fringes. (a) No monochromator, energy width 0.75 eV, (b) with monochromator, slit width 2.5 μm, energy width 0.17 eV and (c) illumination tilted by 30 mrad, monochromator set as for (b).

Table 1
Axial aberration coefficients (for definitions refer to [28]), measuring accuracy (95% confidence interval) and $\pi/4$ limits for different scattering angles. The maximum phase shifts are calculated from the modulus of the measured values or from the precision of the measurement in units of $\pi/4$. The residual phase shift for each aberration coefficient is considered independently.

Aberration coefficient	Measured value	Maximum phase shift at 20 mrad ($\pi/4$)	Maximum phase shift at 27 mrad ($\pi/4$)	Precision (95%-interval) at 27 mrad	Precision of phase shift at 27 mrad ($\pi/4$)
A2	405 nm/71°	1.01	2.48	100 nm	0.61
B2	128 nm/−7°	0.95	2.33	89.7 nm	1.65
C3	−24 μm	0.88	2.93	6.25 μm	0.78
A3	4.8 μm/−106°	0.18	0.60	1.53 μm	0.19
S3	2.9 μm/40°	0.44	1.45	588 nm	0.30
A4	404 μm/51°	0.24	1.08	46 μm	1.07
D4	183 μm/124°	0.54	2.43	29 μm	0.39
B4	112 μm/157°	0.33	1.50	55 μm	0.74
C5	30 mm	0.30	1.81	6.7 mm	0.41
A5	18.7 mm/−89°	0.19	1.12	1.5 mm	0.09

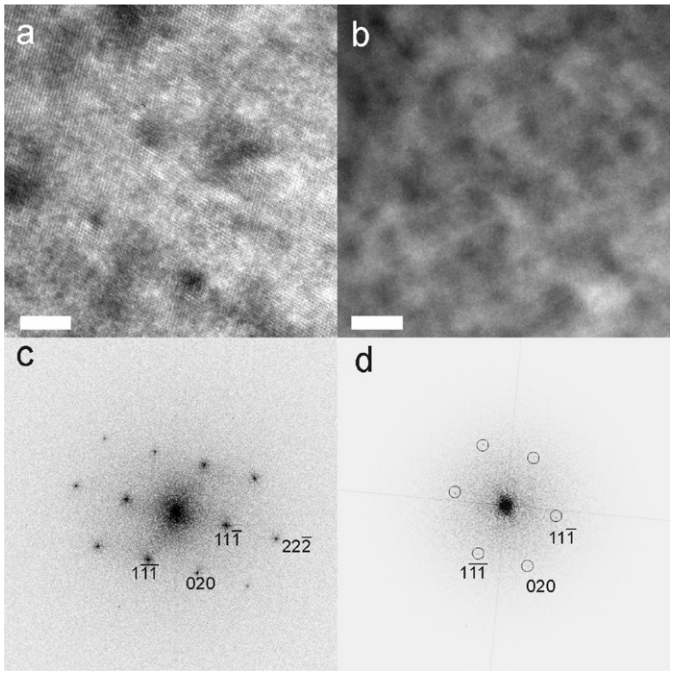

Fig. 2. (a) and (b) HRTEM images of [1 1 0] Si acquired at 20 kV with the prototype *SALVE* instrument, (c) and (d) corresponding FFTs (Fourier transforms). The weak reflections in (d) were encircled to guide the eye. Image (a) was acquired with the monochromator using the 2 μm slit (corresponds to 0.15 eV energy width). Image (b) was acquired with the largest monochromator slit that corresponds to the intrinsic energy width of 0.7 eV of the FEG. Specimen thickness is 4 nm. Scale bars are 5 nm.

small to allow for phase contrast imaging up to 50 mrad (1/0.17 nm at 20 kV).

As a consequence of C_C-correction, the precision of the aberration measurement should improve without further measures for two reasons: with C_C-correction no monochromator is needed. The full current of the electron source can be used which results in a better signal-to-noise ratio. At the same time larger tilts for Zemlin tableaus can be used since tilting hardly influences the information transfer in tilt direction anymore due to the largely reduced focus spread.

3.1.3. Crystalline specimens

In order to judge the HRTEM imaging performance further at 20 kV, we used Si as a well-known self-supporting standard sample. Fig. 2 shows a HRTEM images of [1 1 0] Si, where lattice fringes of 111_{Si} (313.5 pm) and 200_{Si} (271.5 pm) can be clearly seen. The influence of the monochromator on the envelope is demonstrated by comparing the monochromated image (Fig. 1a) with the non-monochromated image (Fig. 2b). Clearly visible lattice fringes are only present in Fig. 2a. However, they can be seen (much weaker) in the Fourier transform of the non-monochromated image as well (Fig. 2d). The 222_{Si} (156.7 pm) reflections can be seen as well in the Fourier transform of Fig. 2c. We assume that they are caused by dynamic diffraction. The high line resolution demonstrates the excellent mechanical and electrical stabilities of the system.

We used single-layer graphene as another test sample for determining the imaging properties of the microscope. Graphene produces a weak signal (compared to most test samples) and is, therefore, visible only if the damping envelopes are reasonably good. The lattice constant of 213 pm corresponds to a scattering angle of about 40 mrad at 20 kV. To overcome limitations caused by chromatic aberrations we employed tilted illumination since the spherical-aberration corrector allows tilting the illumination without causing primary coma and field astigmatism [21,30]. Fig. 3a shows an unfiltered individual exposure from a single-layer graphene membrane, Fig. 3b is corrected for the uneven illumination by background-subtraction. In this example, beam tilt (tilting of 30 mrad) and defocus were adjusted such that all six primary Bragg reflections are present in the Fourier transform (see inset). Fig. 3c represents another example (same sample area as in Fig. 3a) where conditions were optimized (by adjusting defocus and beam tilt azimuth exactly into the direction of one of the $1\bar{1}00$ reflection) to maximize transfer in one of the lattice directions. We have achieved a modulation of 2.5% (of the mean bright-field intensity) at 20 kV for the graphene lattice. The presence of strong graphene lattice fringes confirms a sufficient stability of all components such that a significant portion of the electrons scattered to 40 mrad contribute to the image contrast.

3.1.4. Spectroscopy

For all spectroscopy experiments the TEM was operated in diffraction mode. Fig. 4 shows the low-loss spectrum of Si (collection angle 8.3 mrad, red curve) for VEELS analysis recorded at 20 keV beam energy on the *SALVE* instrument (please note the exceptionary low background noise). The sample thickness was measured to be 10 nm. Reducing the accelerating voltage and the monochromatization in VEELS provides two advantages. First, a strong increase in signal to background ratio is observed by reducing the accelerating voltage and second, the ZLP narrows (energy resolution of 0.11 eV width at half maximum (FWHM)), especially at the full width at one thousandth of the maximum

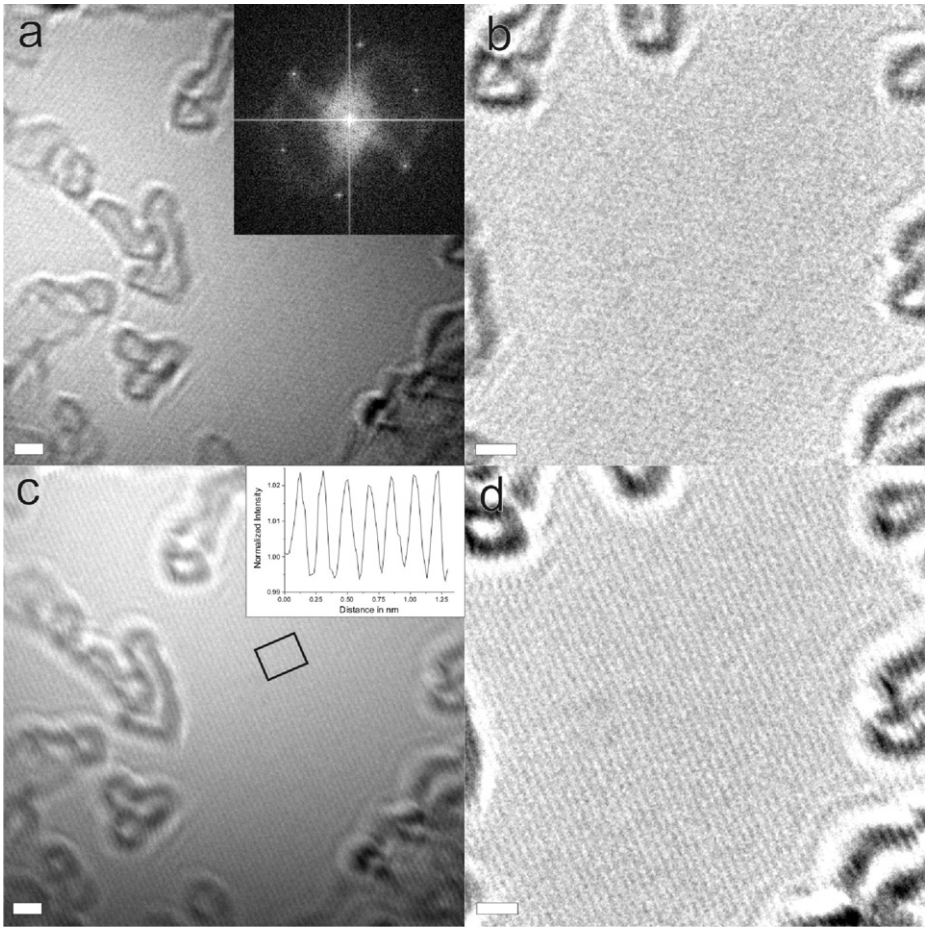

Fig. 3. HRTEM images of single-layer graphene, observed with *SALVE* instrument operating at 20 kV. (a) Unfiltered exposure, with beam tilt and defocus adjusted to transfer all six primary lattice reflections of graphene (corresponding to a 213 pm spacing) with similar intensity. Inset shows Fourier transform of this image. (b) Background-subtracted section of the image (filtered to remove the uneven illumination). (c) Unfiltered single exposure, with conditions adjusted to maximize transfer of one of the lattice reflections. Inset shows that a modulation of 2.5% (normalized to the mean intensity) was achieved. (d) Flat-filtered section of image (c). All scale bars are 1 nm.

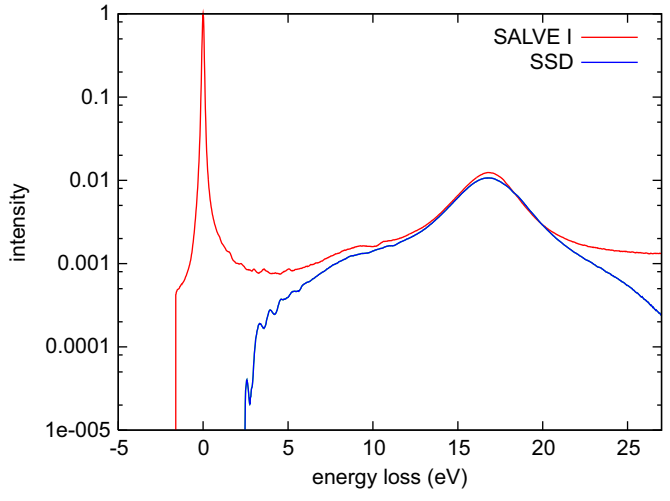

Fig. 4. Low-loss EELS spectra of Si obtained from the *SALVE* instrument operating at 20 kV (solid/red curve), demonstrating the good energy resolution (0.1 eV in vaccum). Please note the logarithmic scaling of the EELS intensity that was necessary to easily display the zero-loss as well as the plasmon losses without cropping the data. Sample thickness: 10 nm. The SSD (dashed/blue line) is the single scattering distribution (SSD) of the spectrum recorded with the *SALVE* instrument. (For interpretation of the references to color in this figure legend, the reader is referred to the web version of this article.)

(FWTM) with 1.0 eV. This is important for accurate band gap determination. Moreover, more spectral details can be observed which are otherwise smeared out (as can be seen in the spectrum in the range from app. 2.6 to 7 eV). Therefore, lowering the accelerating voltage and monochromatization are prerequisite for an accurate determination of the dielectric function of a material. The strong broad feature with its maximum at 9 eV is the surface plasmon followed by the volume plasmon with its maximum at 16.7 eV. The energy range which can be covered by EELS is much larger compared to optical methods (see the blue curve in Fig. 4). For observing weak details in the VEELS spectrum high magnification of the spectrum was chosen at the spectrometer.

For germanium, the collection angle was 8.3 mrad as well. Here the sample thickness was determined to 15 nm. Residual relativistic energy losses were removed off-line by using the iterative routine described in [18].

3.2. Applications of 20 kV TEM

3.2.1. Imaging fullerenes in carbon nanotubes (CNT)

The benefit of imaging radiation-sensitive materials with decreased acceleration voltage is demonstrated by comparison of HRTEM dose series at 80 and 20 kV (Fig. 5) of C_{60} molecules encapsulated within double-walled CNTs. Fullerenes consist of carbon atoms ordered in pentagons and hexagons resulting in

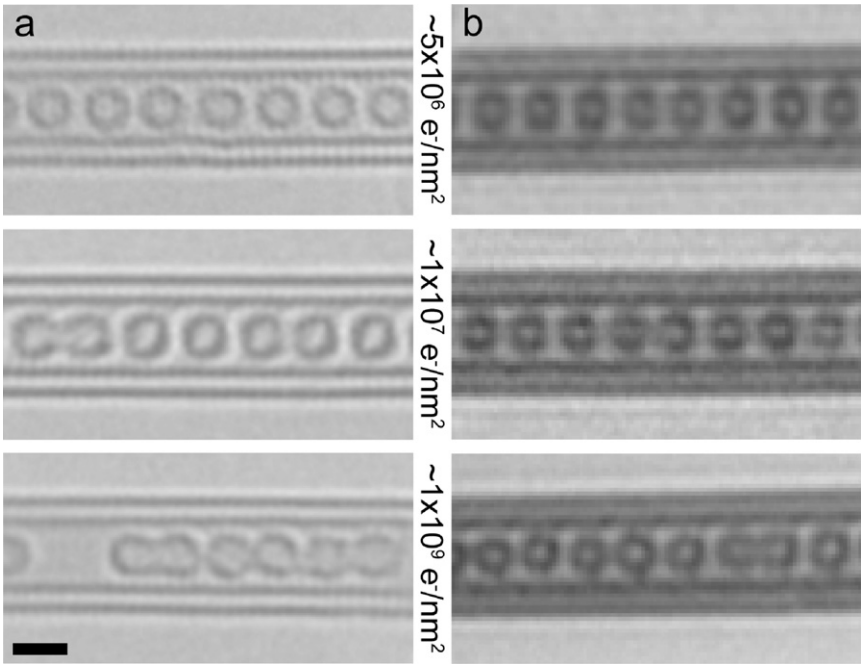

Fig. 5. HRTEM images of C_{60} fullerenes in double-walled CNT at 80 kV (column a) and 20 kV (column b) accelerating voltages representing a dose series with a line-by-line increasing cumulative dose (first row refers to the initial state corresponding to a dose of $\sim 5 \times 10^6$ e$^-$/nm^2). The 80 kV HRTEM experiments serve as a reference showing radiation damage of fullerenes at a dose as low as $\sim 1 \times 10^7$ e$^-$/nm^2; whereas the 20 kV HRTEM images show corresponding damage at $\sim 1 \times 10^9$ e$^-$/nm^2, thus a considerable improvement in e-beam stability in addition to much higher contrast (images were summed up to increase signal-to-noise ratio; scale bar corresponds to 1 nm).

much weaker bonds compared to CNTs, where only hexagons are present. However, the good conductivity of CNTs arising from the delocalized π-electron system slows down radiation damage of molecules encapsulated inside them. Nevertheless, after exposing the C60@DWNT structure to an electron dose of $\sim 1 \times 10^7$ e$^-$/nm^2 at 80 kV, radiation damage effects arise in the form of coalescence and polymerization of the fullerenes. After a cumulative dose of $\sim 1 \times 10^9$ e$^-$/nm^2, almost all molecules got damaged at 80 kV and started coalescing to form a third nanotube within the DWNT. In contrast, at the same dose at 20 kV only very few structural changes were observable. This indicates that the electron beam damage is reduced at 20 kV by a factor of approximately 100 times compared to 80 kV. In addition, the images at 20 kV show, in accordance to theory, much higher contrast. However, at present the resolution of the atomic lattice of the molecules and nanotubes is limited by chromatic aberration at such low voltages. In future these limitations will be eliminated by means of the new C_C/C_S corrector installed in the final *SALVE* instrument.

3.3. Valence EELS of Si and Ge

3.3.1. Silicon

We have determined the direct band gap of 2.6 eV for Si after ZLP and plural scattering removal. This value is in very good agreement with band structure calculations [31]. Application of KKA provided the complex dielectric function and the energy loss dependent refractive index for Si, as depicted in Fig. 6, red curve. The comparison with optical measurements taken from Ref. [30] (green crosses) shows a very good agreement with two exceptions: the energy range of the broad surface plasmon peak around 9 eV and the sharp feature at 4.5 eV. The reason for the first discrepancy (around 9 eV) is surface oxidation of the silicon specimen in our experiment, whereas the optical data was recorded under ultra-high vacuum conditions preventing surface oxidation. The reason for the absence of the sharp feature at 4.5 eV in our experiment is not clear so far. It might be connected to the fact that

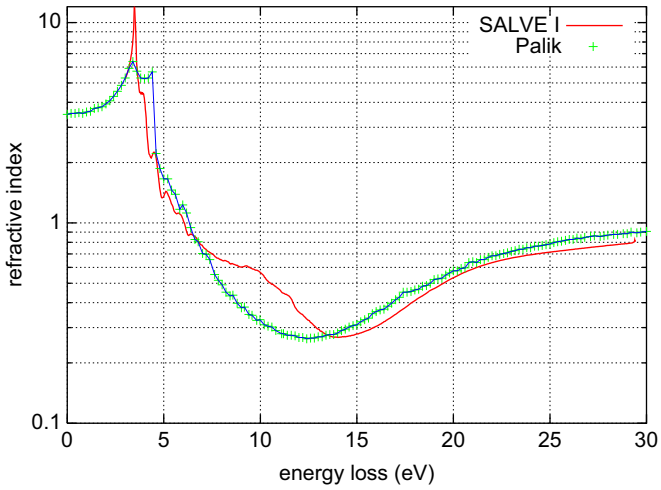

Fig. 6. Refractive indices over energy loss obtained (solid/red curve): from the VEELS spectra shown in Fig. 3 after corresponding KKA analysis and (crossed/green curve): from the optical data presented by Palik in Ref. [36]. (For interpretation of the references to color in this figure legend, the reader is referred to the web version of this article.)

the surface plasmon is shifted to lower energies due to the presence of silicon oxide on the specimen surface. This shift introduces an error when the KKA routine treats the surface plasmon. The result represents therefore the mean dielectric function of the non-oxidized bulk and the oxidized surfaces.

3.3.2. Germanium

Calculations show that in the case of Ge, an electron probe with only 5 kV would be necessary to avoid relativistic energy losses [18]. Our experiment demonstrate that an energy of 20 kV already allows a high signal-to background ratio in the band gap region of the VEELS, which might be caused by a reduction of

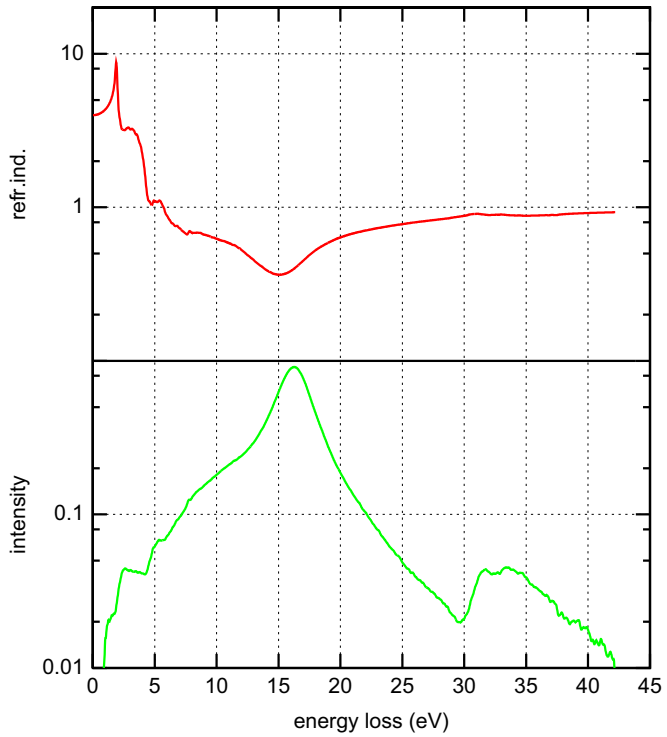

Fig. 7. Bottom: single scattering distribution of Ge obtained at 20 keV electron energy with the *SALVE* instrument as a function of the energy loss. The direct band gap is measured to be (0.80 ± 0.03) eV. Top: refractive indices over energy loss obtained from the VEELS spectrum shown in Fig. 6 after corresponding KKA analysis.

relativistic losses. An iterative routine [18,32] was employed to determine this result. Subsequently, we calculated the refraction index as a function of the energy loss by applying KKA. Note that the refraction index was derived even for high energy losses, where optical measurements fail. Fig. 7 shows the single scattering distribution (SSD) of germanium recorded with the *SALVE* instrument at 20 kV. After subtraction of the zero-loss peak, the direct band gap is measured to be (0.80 ± 0.03) eV. This result is in excellent agreement with those obtained from optical measurements and band structure calculations [33,34].

The obtained refractive index is in excellent agreement with earlier work [35]. However, the transition strengths are different compared with those obtained from optical methods [30] and calculations based on density functional theory. The reason for this discrepancy is not clear yet and needs more detailed study of the influence of the collection semi-angle on band bending.

4. Conclusion

We have characterized the new prototype *SALVE* instrument at 20 kV operation, which is based on the Zeiss-Libra200 platform including an in-column energy filter and is equipped with an electrostatic monochromator and a C_S-corrector from CEOS. We have shown that the high stability of the microscope allows high contrast imaging resolving lattice fringes in 4 nm thin Si lamellae directly up to 271.5 pm (Si {002}) and in single-layer graphene up to 213 pm (graphene $\{1\bar{1}00\}$, tilted illumination) at 20 kV.

In high-resolution imaging mode we showed that at 20 kV fullerenes encapsulated within carbon nanotubes withstand a 100 times larger electron dose than at 80 kV before any significant damage in their structures can be noticed. In spectroscopy mode we show that optical properties can be determined at 20 kV in nearly all materials. Something that is not possible at higher voltages because of much lower signal to background in the VEELS region of the spectra, caused most probably by relativistic energy losses. We determined, for the first time by means of TEM, the band gap and the refractive index of Si and Ge as functions of the energy loss. The obtained results are in very good agreement with data from optical measurements. We may note that surface plasmons in the low-loss region of the EELS spectrum may be increased because the sample thickness must be reduced for 20 kV. Nevertheless, it is now possible to determine optical properties in a much wider energy loss region than accessible by optical spectroscopy.

The final *SALVE*-instrument equipped with C_C/C_S corrector and an optimized detector will allow atomic resolution imaging and spectroscopy of radiation-sensitive objects in the near future.

Acknowledgment

We gratefully acknowledge financial support by the German Research Foundation (DFG) and the Ministry of Science, Research, and Arts (MWK) of the state Baden-Württemberg within the Sub Angstrom Low-Voltage Electron Microscopy (*SALVE*) project.

References

[1] H. Rose, Outline of a spherically corrected semiaplanatic medium-voltage transmission electron microscope, Optik 85 (1990) 19–24.
[2] H. Rose, History of aberration correction, Advances in Imaging and Electron Physics 156 (2008) 1–36.
[3] M. Haider, H. Rose, S. Uhlemann, E. Schwan, B. Kabius, K. Urban, A spherical-aberration corrected 200 kV transmission electron microscope, Ultramicroscopy 75 (1998) 53–60.
[4] B. Kabius, P. Hartel, M. Haider, H. Müller, S. Uhlemann, U. Loebau, J. Zach, H. Rose, First application of C_c-corrected imaging for high-resolution and energy-filtered TEM, Journal of Electron Microscopy 58 (2009) 47–155.
[5] R.F. Egerton, R. McLeod, F. Wang, M. Malac, Basic questions related to electron-induced sputtering in the TEM, Ultramicroscopy 110 (2009) 991–997.
[6] H. Rose, Future trends in aberration-corrected electron microscopy, Philosophical Transactions of the Royal Society A 367 (2009) 3809–3823.
[7] A.P. Wilska, Low-voltage electron microscopy, a 6 kV instrument, Journal of Royal Microscopical Society 83 (1964) 207–211.
[8] U. Kaiser, A. Chuvilin, J.C. Meyer, J. Biskupek, Microscopy at the bottom, in: W. Grogger, F. Hofer, P. Poelt (Eds.), Materials Science Microscopy Conference MC2009, vol. 3, 2009, pp. 1–6.
[9] H. Sawada, T. Sasaki, F. Hosokawa, S. Yuasa, M. Terao, M. Kawazoe, T. Nakamichi, T. Kaneyama, Y. Kondo, K. Kimoto, K. Suenaga, Higher-order aberration corrector for an image-forming system in a transmission electron microscope, Ultramicroscopy 110 (2010) 958–961.
[10] O.L. Krivanek, N. Dellby, M.F. Murfitt, M.F. Chisholm, T.J. Pennycook, K. Suenaga, V. Nicolosi, Gentle STEM: ADF imaging and EELS at low primary energies, Ultramicroscopy 110 (2010) 935–945.
[11] L.A. Giannuzzi, J.L. Drown, S.R. Brown, R.B. Irwin, F.A. Stevie, Applications of the FIB lift-out technique for TEM specimen preparation, Microscopy Research and Technique 41 (1998) 285–290.
[12] R.M. Langford, Focused ion beams techniques for nanomaterials characterization, Microscopy Research and Technique 69 (2006) 538–549.
[13] A.K. Geim, K.S. Novoselov, The rise of graphene, Nature 6 (2007) 183–191.
[14] J.C. Meyer, C. Kisielowski, R. Erni, M.D. Rossel, M.F. Crommie, A. Zettl, Direct imaging of lattice atoms and topological defects in graphene membranes, Nano Letters 8 (2008) 3582–3586.
[15] M. Stöger-Pollach, Low voltage TEM: influences on electron energy loss spectrometry experiments, Micron 41 (2010) 577–584.
[16] M. Stöger-Pollach, et al., Cerenkov losses: a limit for bandgap determination and Kramers–Kronig analysis, Micron 37 (2006) 396–402.
[17] M. Stöger Pollach, Optical properties and band gaps from low loss EELS: pitfalls and solutions, Micron 39 (2008) 1092–1110.
[18] K. Suenaga, Y. Sato, Z. Liu, H. Kataura, T. Okazaki, K. Kimoto, H. Sawada, T. Sasaki, K. Omoto, et al., Visualizing and identifying single atoms using electron energy-loss spectroscopy with low accelerating voltage, Nature Chemistry 1 (2009) 415–418.
[19] A. Chuvilin, A.N. Khlobystov, D. Obergfell, M. Haluska, S. Yang, S. Roth, U. Kaiser, Observations of chemical reactions at the atomic scale: dynamics of metal-mediated fullerene coalescence and nanotube rupture, Angewandte Chemie International Edition 49 (2010) 193–198.
[20] S. Uhlemann, M. Haider, Experimental set-up of a fully electrostatic monochromator for a 200 kV TEM, in: J. Engelbrecht, T. Sewell, M. Witcomb,

R. Cross, P. Richards (Eds.), Proceedings of 15th International Congress on Electron Microscopy vol. I, Microscopy Society of Southern Africa, Durban, 2002, p. 327.
[21] M. Haider, P. Hartel, H. Müller, S. Uhlemann, J. Zach, Information transfer in a TEM corrected for spherical and chromatic aberration, Microscopy and Microanalysis 16 (2010) 393–408.
[22] L. Lechner, J. Biskupek, U. Kaiser, Methode und Apparate zur Präparation von TEM-Proben, German patent # P18420DE.
[23] K.S. Kim, Y. Zhao, H. Jang, S.Y. Lee, J.M. Kim, K.S. Kim, J.-H. Ahn, P. Kim, J.-Y. Choi, B.H. Hong, Large-scale pattern growth of graphene films for stretchable transparent electrodes, Nature 457 (2009) 706.
[24] X. Li, W. Cai, J. An, S. Kim, J. Nah, D. Yang, R. Piner, A. Velamakanni, I. Jung, E. Tutuc, S.K. Banerjee, L. Colombo, R.S. Ruoff, Large-area synthesis of high-quality and uniform graphene films on copper foils, Science 324 (2009) 1312.
[25] H.J. Park, J.C. Meyer, S. Roth, V. Skakalova., Growth and properties of few-layer graphene prepared by chemical vapor deposition, Carbon 48 (2010) 1088.
[26] F. Wang, R.F. Egerton, M. Malac, M., Fourier-ratio deconvolution techniques for electron energy-loss spectroscopy (EELS) original research article, Ultramicroscopy 109 (2009) 1245–1249.
[27] P. Schattschneider, A performance test of the recovery of single energy loss profiles via matrix approach, Ultramicroscopy 11 (1983) 321–322.
[28] S. Uhlemann, M. Haider, Residual wave aberrations in the first spherical aberration corrected transmission electron microscope, Ultramicroscopy 72 (1998) 109–119.
[29] H. Müller, I. Maßmann, S. Uhlemann, P. Hartel, J. Zach, M. Haider, Aplanatic imaging systems for the transmission electron microscope, Nuclear Instruments and Methods A, in press, doi:10.1016/j.numa.2010.12.091.
[30] R.R. Meyer, A.I. Kirkland, W.O. Saxton, A new method for the determination of the wave aberration function for high-resolution TEM: 2. Measurement of the antisymmetric aberrations, Ultramicroscopy 99 (2004) 115123.
[31] D.J. Moss, E. Ghahramani, J.E. Sipe, H.M. van Driel, Band-structure calculation of dispersion and anisotropy for third-harmonic generation in Si, Ge, and GaAs, Physical Review B 41 (1990) 1542–1560.
[32] E.D. Palik, Handbook of Optical Constants of Solids, Orlando, FL, US, 1985–1991.
[33] M. Stöger-Pollach, A. Laister, P. Schattschneider, Treating retardation effects in valence-EELS spectra for Kramers Kronig analysis, Ultramicroscopy 108 (2008) 439–444.
[34] R.P. Seysan, A.V. Varfolomeev, B.P. Zaharchenya, Properties of semiconductors, Fizika i Tekhnika Poluprovodnikov 2 (1968) 1276–1280.
[35] J. Kim, M.V. Fischetti, Electronic band structure calculations for biaxially strained Si, Ge, and III–V semiconductors, Journal of Applied Physics 108 (2010) 0113710.
[36] H.R. Philipp, E.A. Taft, Optical constants of germanium in the region of 1 to 10 eV, Physical Review 113 (1959) 1002–1005.
[37] E.E. Fill, F. Krausz, M.G. Raizen, Single-molecule electron diffraction imaging with charge replacement, New Journal of Physics 10, 093015.